Weathering of earth-painted surfaces:

Environmental monitoring and artificial aging

Marta Cappai[1], Ludovica Casnedi[1], Gianfranco Carcangiu[2], Francesco Delogu[1], Denise Pozzi-Escot[3], Gianella Pacheco Neyra[3],Giorgio Pia[1]*, Paola Meloni[1]

[1] Dipartimento di Ingegneria Meccanica, Chimica e dei Materiali, Università degli Studi di Cagliari, Piazza d'Armi, 09123 Cagliari, Italy.

[2]Institute of AtmosphericSciences and Climate ISAC, CNR, Via Piero Gobetti 101, Bologna 40129, Italy

[3] Museo Pachacamac, Antigua Carretera Panamericana Sur Km. 31.5, Distrito de Lurín, Lima

* Corresponding author: Giorgio Pia, giorgio.pia@unica.it, telephone +390706755051, fax +390706755067

Abstract

Relating damage development to the specific environmental conditions is of paramount importance to design effective conservation strategies for archaeological and historical sites. For this reason, artificial weathering is a highly debated topic in materials science applied to Cultural Heritage. In this work, we report on the weathering of decorated earthen plasters from *Templo Pintado* in *Pachacamac* (Region of Lima, Peru) and define a methodology to accelerate aging of painted raw earth surfaces. Weathering was simulated by exposing the surfaces to wet-dry and sandblasting cycles and resulting damage was estimated via the amount of material removed from the original surface. The results are in agreement with weathering dynamics observed in situ, which allows designing suitable methodology for the preparation of samples to be used in testing procedures addressing the preservation of surfaces.

Keywords: Accelerated aging, archaeological surfaces, earthen plaster, natural weathering.

1. Introduction

Raw earth is, by far, one of the most widely used materials by mankind throughout the ages and in all hemispheres to construct homes, buildings and cities. Its presence gives us continuity between the present and the past. It is still one of the most widely used materials: it is estimated that even today about 50% of the population lives in the buildings made from this material [1]. Evidence of the past has come down to us in the form of buildings and towns that are now an important part of our archaeological and cultural heritage [2–6]. Some of these testimonies are also enriched and embellished by the examples of wall paintings made with different coloured earths, which are often a fundamental element in improving our understanding of cultures far away in time [7–10]. Currently, more than 180 sites of the UNESCO World Heritage List [11–13] are fully or partially built in raw earth. Unfortunately, about 25% of such sites are also included in the UNESCO World Heritage in Danger List owing to their extreme sensitivity to the atmospheric agents [2,6,14,15].

Combined with its inherent complexity [16], the propensity of raw earth to weathering calls for constant maintenance of earthen architectures [5,17–19]. Unfortunately, at archaeological sites, maintenance operations were interrupted hundreds of years, with the consequent, unavoidable deterioration of structures and surfaces. In addition, the excavation operations expose the archaeological structures to significant thermo-hygrometric shock, which accelerates their degradation [3,9,10]. At present, only effective *conservation*, *restoration* and *protection* strategies can allow depressing degradation rates and preserving historical evidences.

In the case of painted surfaces, the several deterioration processes are pulverization, peeling and flaking as well as different types of fracturing mostly due to the action of water in all its forms [8,10,17,20] and the preservation requires consolidation and re-adhesion operations [21].

Accordingly, inorganic and organic materials with aggregating properties are applied to deteriorated surfaces by impregnation or injection to enhance the cohesion of pictorial layers

and their adhesion to the support [20]. Nevertheless, consolidation of earth-painted surfaces is still an open issue [22]. Although a vast literature debates on the use of consolidants on earth surfaces [3,23,24], information concerning earth paintings is scarce [18,22,25–27]. In several cases, the lack of reliable evidence on the effects induced by the use of given consolidants has even worsened the deterioration process in the long term [26,28]. It follows that finding a suitable solution to avoid, or at least limit, damage caused by consolidant aging is highly desirable [29,30].

In this respect, consolidants for earthen surfaces should be tested before their application on original surfaces [31]. For non-decorated surfaces, it is possible to sample very small amounts of material and evaluate the effects of consolidants on the original surfaces [21,32]. Sampling is not recommended for decorated surfaces [33], so that surfaces expressly built to mimic original ones are typically used in experimental tests [26,34,35]. In this case, to avoid unrealistic outcomes stemming from non-deteriorated surfaces, newly built surfaces are subjected to accelerated aging [36]. Accordingly, suitable methods are utilized to reproduce in short time the processes nature operates on very long time scales [37–39].

Literature is relatively rich in this regard [40–47]. In most cases, the methods consist of destructive tests that do not allow re-using the specimens to evaluate consolidation efficiency [36]. Less frequently, artificial aging is designed to reproduce the damage suffered by real surfaces from atmospheric agents [42] through wet-dry cycling [25,48] or mild mechanical solicitation [49–51]. One of the difficulties raised in this latter case is that the intimate relationship between environmental parameters and deterioration requires a case-sensitive assessment of the accelerated aging methodology.

Considering all the above, this work focuses on the painted surfaces of the *Templo Pintado* in the archaeological site of *Pachacamac*, located in the coastal region of Peru [52].

First, the environmental data collected in situ were studied and correlated with surface degradation pathologies. In specific portions of the painted surfaces of the *Templo Pintado*, the degree of cohesion and adhesion was evaluated by Scotch Tape Test (STT) measurements. Subsequently, some plaster fragments were characterised in the laboratory and similar soils were chosen to reproduce them. Then, an artificial aging methodology based on wet-dry and sandblasting cycles has been presented. The degree of the obtained weathering shows data in agreement with experimental ones acquired in situ and allows to have reliable samples for testing new preservation approaches.

2. The archaeological site

The Archaeological Sanctuary of *Pachacamac* (Region of Lima, Peru) was one of the most important oracles and destinations of pilgrimage in the central Peruvian coast for more than 1000 years (200 - 1533). *Pachacamac* was a deity of the ancient Incas pantheon. Son of the Sun god, he was believed to be the god of fire and to have rejuvenated the world originally created by Viracocha. Incas defined him as *He who moves Earth* [53], thus interpreting the fearful earthquakes affecting Peru as an expression of his wrath.

The *Pachacamac* site covers an area of about 465 hectares in the desert. It is located about 31 km South-East of Lima, in the lower part of the Lurin Valley. The climate is hot arid/humid, typical of subtropical coastal areas, and it is characterised by extremely reduced rainfall, high relative humidity and prevailing South/South East winds with speeds generally ranging from 9.6 km h^{-1} to 13.6 km h^{-1} with spikes in summer up to 35 km h^{-1}[54]. Environmental data recorded *in situ* for four years by the *Davis Vantage Pro 2* weather station revealed that average temperature is around 22 °C in summer and 16 °C in winter, with temperature fluctuations between day and night of about ± 4 °C. Relative humidity is 90% ± 6%, with highest values recorded during the night. Rarely, in the Autumn and Spring months, it can take lower values around 85% ± 3%. From August to September, strong winds blow from North-East coming from the coast located at 4 km, with peaks of 35 km h^{-1}, and affecting the so-called *Frontis Norte* (*FN*) of *Templo Pintado*. In summer days, solar radiation reaches values of 7.90 kW h/m^2 in a few hours.

Presently, the area includes more than 50 structures from different historical periods and built with different techniques and materials [55,56]. The *Templo Pintado* is one of them.

The *Templo Pintado* is situated in the north-centre part of the Sacred Precinct and consists of a rectangular structure built in adobe with stepped walls and a total surface area of about 120×65 m^2. It is the only building within the Sanctuary area that exhibits polychrome mural paintings. Mostly located on the *FN*, a picture of which is shown in Fig. 1a, mural paintings were used to distinguish the house of the deity from the rest, thus allowing the pilgrims entering the Sanctuary to enjoy the celebration of *Pachacamac* power [54,57].

Templo Pintado's paintings have been created on an earthen plaster of variable thickness. Due to continuous maintenance, plasters and pictorial layers have been renewed several times

and they are stratified. Sometimes, they have been simply refreshed, a sort of maintenance when drawings got almost completely erased. In other cases, a new, thin layer of plaster was applied and the drawings were renewed or changed, as evident from Fig. 1b [54]. The pictorial method used was temple mate. Garnet red, ochre yellow, vermilion red, pale yellow, black and green are well recognisable colours, with vermilion red and pale yellow being the predominant colours on the surfaces of *FN*.

Fig. 1 - (a) Detail of Frontis Northe of Templo Pintado; (b) Sample of archaeological plaster of Templo Pintado.

After the Spanish conquest, the *Templo Pintado* was gradually abandoned and buried by desert sand, which allowed its conservation for about 400 years. The temple became exposed again to atmospheric agents in 1939, when excavations began [58], and only in 2008, an international research programme started a systematic conservation activity on the main structure and mural paintings [54].

Decorated surfaces have been exposed to weathering and anthropic factors for over 70 years, causing the loss of valuable archaeological information. Degradation of paintings is mostly related to temperature and relative humidity variation along with solar irradiation and

wind exposure. Day by day, clay components of the earth paintings undergo swelling and contraction, eventually causing pulverization, chalking, peeling, flaking and cracking of decorated surfaces. The composition of different pictorial layers determines which degradation process prevails on the others. For instance, pale yellow surfaces are mostly affected by pulverization, while red vermillion surfaces mostly suffer from flaking.

The strong winds significantly erode the loosely bound layers of decorated surfaces, particularly along the *FN* during the summer season. In addition, they mediate *saltation*, i.e. the mass transport of sand particles from the desert around the *Templo Pintado*. Typically, the particles involved have diameter between 0.1 and 0.5 mm [59], and they can hit the decorated surfaces at a height of up to 120 cm, although most of them do not go above 30 cm. The steps of *Templo Pintado* are 40 to 120 cm high and dust and sand accumulate easily on each tread of the steps, contributing to its erosion by frictional processes. To mitigate such phenomena, a removable shelter was also constructed in 2010.

3. Materials and Methods

3.1 Archaeological surfaces

Seven pale yellow and six vermilion red portions of painted plaster in the *FN* such as those shown in Fig. 2 were chosen to evaluate the degree of cohesion and adhesion among different layers/plasters. All the fragments investigated come from the *sector 1* of *FN* and have undergone similar exposure to atmospheric agents and similar state of preservation. Tests were carried out according to the so-called Scotch Tape Test (STT) described by Ferron [35] and Malpartida [60], and inspired by ASTM 4214-07 [61]. A 3M® Scotch® 550 tape in polypropylene with acrylic adhesive was used. Portions with a 40×19 mm^2 surface area were cut, gently applied to the surface and leaned on for 90 seconds. Then, they were removed at the constant speed of 10 mm s^{-1} at an angle of 90° and placed on a sheet of white photo paper. In order to estimate the fractional area occupied by particles removed from the sample, the tape surface was acquired using Epson® image scanner and the obtained images were analysed using the ImageJ® 1.46 software. STT can be strongly influenced by extremal fluctuations of relative humidity and temperature due to the sensitivity of the test material and the tape adhesive layer . Thus, it is highly desirable to maintain similar values of temperature and relative humidity [62]. For this reason, measurements were performed during the spring

season, when temperature and relative humidity undergo reduced excursion. The measurement campaign was carried out from 9 to 10 am with an average T of 16.5°C and an average RH of 88%.

Fig. 2 - Two of the pictorial fragments on which monitoring and STT were carried out: pale yellow (a) and vermilion red (b).

For each painted portion studied, 3 measurements were taken at different points with diverse tape orientation on the surface (21 measurements for each colour). The obtained data were then averaged, for each surface, to have a more representative value. Final data were obtained averaging over the seven surfaces having the same colour. For pale yellow surfaces, the average value relative to the seven surfaces is 26.93%, with a maximum value of 28.93% and a minimum value of 25.02%. For vermilion red surfaces, the average value is 13.70%, with a minimum value of 12.17% and a maximum value of 15.97%. Such values have been used as the reference for accelerated aging in the laboratory. Furthermore, in the case of pale yellow, the material removed from the tape was dust, indicating a pulverization due to the lack of cohesion between the particles of the layer. In the case of vermillion red, the removed material consisted of small flakes, indicating a lack of adhesion between the surface layer and the underlying one. Differences in the two degradation forms affect the evidence obtained via

STT. In fact, for pale yellow surfaces, the maximum deviation recorded between the three measurements for each surface is 0.8%, while it is 1.5% for vermillion red surfaces. The measurements carried out on pale yellow surfaces appear more uniform because of the greater homogeneity of the surface affected by pulverisation. For vermilion red surfaces, which are themselves more cohesive but subject to detachment from the underlying layers, the flakes of pictorial layer are removed from the surface mostly where micro-cracks and weaknesses are present. Flake removal results in larger fluctuations in measurements..

3.2 Archaeological samples

Fragments were collected from the excavation of the *FN* performed in 2014. The mineralogical composition of mortar plaster and painted layers was determined by X-ray diffraction (XRD) using a Rigaku MiniFlex II diffractometer. XRD patterns were analysed taking advantage of the X'Pert software and the Rietveld method [63]. The qualitative identification and characterisation of clay minerals were performed on a plaster mortar, consisting of (*i*) concentration of the clay fraction, (*ii*) exposure to an atmosphere saturated with ethylene glycol for 8 hours at 60°C and (*iii*) muffle furnace at 550°C for 2 hours [64]. It was not possible to perform the same qualitative characterisation of the clays on the pictorial layers due to the small amount of samples available. The results of XRD analyses are shown in Tab. 1. Albite is, invariably, the predominant crystalline phase. An analysis of the weight fractions of the plaster mortar shows that the amount of clay present is about 3% and its qualitative interpretation reveals the presence of a smectitic clay, which makes the plaster particularly susceptible to hygrometric variations caused by the changes in the humidity inside the material. The earth used for the pale yellow surfaces shows that the mineral to which the typical colouring can be ascribed is Jarosite. The quantitative analysis shows the presence of clay species belonging to the chlorite group in weight percentages of 2%. The analysis also clearly identified a high % (approximately 13%) of a clay mineral belonging to the Illite group. Finally, in the case of the earth used for the vermilion red surfaces, the colour is given by the presence of haematite, about 2%. The clay species present belong to the group of chlorites and illites in total weight percentages of about 14.5 %.

Tab. 1 - Mineralogical composition (MC) of the archaeological earthen plaster and pictorial layers; Mohs value (MV) of different minerals in archaeological painted surfaces.

Mortar	**Pale yellow**		**Vermillon red**	
MC	**MC**	**MV**	**MC**	**MV**
Albite: 51.07 ± 2.01	Albite: 40.27 ± 1.45	6.25	Albite: 35.17 ± 2.57	6.25
Clinochlore: 2.98 ± 0.12	Clinochlore: 1.90 ± 0.16	3.00	Gypsum: 1.61 ± 0.06	2.00
Hornblende: 4.33 ± 0.14	Gypsum: 0.90 ± 0.02	2.00	Hematite: 2.25 ± 0.14	6.50
Laumontite: 3.04 ± 0.42	Illite: 12.78 ± 0.80	1.50	Illite: 11.84 ± 1.95	1.50
Muscovite: 1.79 ± 0.09	Jarosite: 31.81 ± 0.84	3.50	Muscovite: 15.28 ± 4.44	2.25
Orthoclase 19.44 ± 0.98	Kozulite: 3.25 ± 0.12	5.00	Orthoclase: 6.99 ± 1.06	6.00
Quartz: 17.34 ± 0.03	Quartz: 9.08 ± 0.05	7.00	Quartz: 23.31 ± 0.07	7.00
			Riebeckite: 0.35 ± 0.03	6.00
Sigma: 2.20	Sigma: 1.93		Sudoite: 2.33 ± 0.15	3.00
Rwp%: 14.54	Rwp%: 16.70		Wollastonite: 0.86 ± 0.62	4.75
			Sigma: 1.34	
			Rwp%: 9.59	
Clay minerals group– qualitative identification				
Illite Chlorite Smectite	--		--	

Particle size of mortar plaster was determined by humid granulometry [63,64]. The obtained curve (Fig. 3a) follows a rather vertical trend, indicating uniformity in the size of the grains belonging to the fine sands, which are the most abundant granulometric fractions of the earth. The percentage of retained earth in different sieves showed that the mortar mixture is mostly made up of particles with a diameter between 0.250 cm and 0.125 cm (45%), thus a mortar is characterised by a high fine sand content. The fine fraction passing ø 0.063 cm, consisting of silt and clay particles, is 27% and is the second most abundant fraction. In the larger diameter fractions, i.e. 2 to 0.5 mm, numerous shell fragments are present due to the fact that the site is located on the coastal strip and the materials used for plastering and construction were found locally or in a restricted geographical area. Due to the small amount of sample available, such analysis was not possible for painted layers.

3.3 Earth materials for samples

The mineralogical composition of earths is known to exhibit remarkable elements of uniqueness. Materials taken from different geographical areas, even close to each other, usually have completely different mineralogical composition, which greatly complicates any comparative analysis, making it virtually impossible to prepare test samples fully comparable with historical earth materials.

Since weathering is mostly caused due to wind erosion and thermal-hygrometric excursion, a rational strategy to enable a meaningful comparison is to select the earth material to be used for preparing test samples based on the hardness of the mineralogical phases and similar typologies of clay minerals. Indeed, such characteristics influence durability performance of the plaster and painted surfaces [65].

In our case, historical earthen materials have mineralogical composition characterised either by a relatively large fraction of quartz and smaller fractions of clay minerals or by a comparable amounts of such two components. Accordingly, two different earths available in Sardinia (Italian region) to simulate the plaster used by different Cultures of *Pachacamac* were chosen. The first earthen material, hereafter denoted as named TN, was collected from the Nurachi area in the province of Oristano. The second earth, hereafter denoted as VNF, was collected from the territory between Villanovafranca and Isili. The earths mentioned above, selected to be used for support, were characterised by XRD with the same procedure as discussed for archaeological samples, humid granulometry and Atterberg limits.

The resulting mineralogical compositions are reported in Tab. 2. It can be seen that the principal mineralogical phase is quartz. TN shows a little amount of smectite clay, which can also be found in the plaster samples taken from *Templo Pintado*. VNF earth has a high calcium carbonate content due to its pedogenetic process on marl soils and shows clay minerals belonging to the illite and chlorite groups.

Tab. 2 - Mineralogical composition of TN and VNT.

Mineralogical composition of TN and VNT	
TN	**VNF**
Albite 35.93 ± 2.34	Biotite: 0.61 ± 0.09
Anorthite: 41.51 ± 4.03	Calcite: 45.78 ± 0.03
Hematite: 1.21 ± 0.25	Muscovite 10.42 ± 0.44
Illite: 1.23 ± 0.22	Orthoclase: 28.52 ± 1.28
Kaolinite 3.27 ± 0.13	Quartz: 11.79 ± 0.41
Muscovite 2.69 ± 0.28	Sudoite: 2.88 ± 0.13
Quartz: 14.16 ± 0.04	
Sigma: 1.70	Sigma: 1.44
Rwp%: 11.34	Rwp%: 12.70
Clay minerals group– qualitative identification	
Kaolinite	Chlorite
Smectite	Illite

The particle size distributions obtained by humid granulometry [63,64] are shown in Fig. 3b. The TN earth consisted of approximately 89% of particles passing through the sieve with a mesh opening of 0.063 mm (silt and clay), with a very low percentage of sand (approximately 10% adding the percentages of coarse, medium and fine sand) and the total absence of particles larger than 4 mm. The VNF Terra consists of approximately 82% of particles passing through the 0.063 mm sieve (silt and clay). It also has a low percentage of sand (18% between coarse, medium and fine sand) and a total absence of particles larger than 4 mm. The data reveal a greater granulometric assortment of the material characterised by a slightly more consistent sandy skeleton than in the case of TN soil.

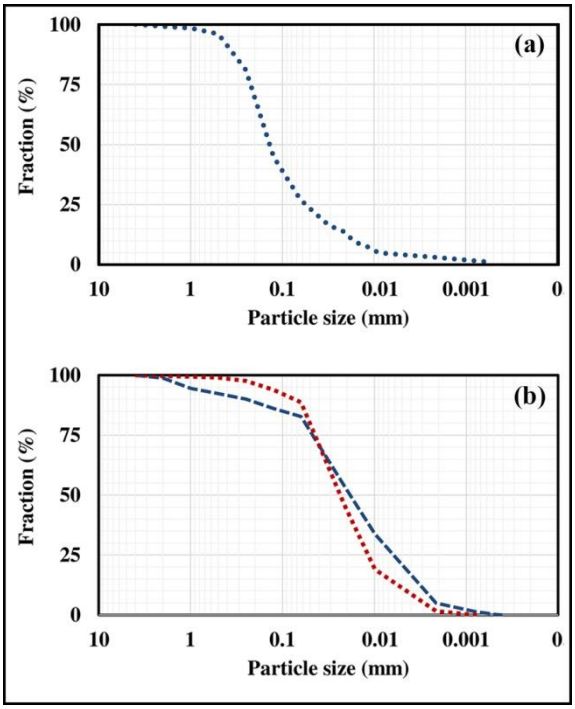

Fig. 3 - (a) Particle size distribution of TN (blue) and VNF (red). (b) Particle size distribution of archaeological earthen plaster.

The Atterberg limits [65] show an IP value of 20% for the TN sample, which therefore places it in the range of plastic soils with a good propensity to be worked, while VNF, with an IP value of 13%, is in the range of soils with low plasticity. The results obtained are given in Tab. 3.

Tab. 3 - Atterberg limits of TN and VNT.

Atterberg limits	
TN	**VNF**
w_L= 45%	w_L= 35%
w_P= 25%	w_P= 22%
IP= 20%	*IP*= 13%
w_s= 23.14%	w_s= 17.98%

Pictorials layers were prepared by grinding earth or stone fragments. Particle size was selected below 0.063 mm using suitable mechanical sieving. A Sardinian earth sampled in the territory of Serrenti was used for yellow finishing, hereafter denoted as FIN_Y. In contrast, pink finishing, hereafter denoted as FIN_P, was obtained by grinding fragments of sedimentary rock taken from a quarry in the *Pachacamac* site. The mineralogical composition of these finishings is shown in Tab. 4.

Tab. 4 - Mineralogical composition (MC) of FIN_Y and FIN_P and Mohs value (MV) of different minerals.

FIN_Y		**FIN_P**	
MC	**MV**	**MC**	**MV**
Albite 7.10 ± 0.72	6.25	Albite 16.46 ± 2.80	6.25
Dickite 1.60 ± 0.25	2.75	Calcite: 3.64 ± 0.29	3.00
Kaolinite 0.96 ± 0.25	2.25	Clinochlore: 2.28 ± 0.20	3.00
Muscovite 4.03 ± 0.48	2.25	Kaolinite 0.70 ± 0.08	2.25
Orthoclase: 2.45 ± 0.33	6.00	Muscovite 7.95 ± 0.83	2.25
Quartz: 83.85 ± 0.08	7.00	NaCl 1.11 ± 0.05	2.00
		Quartz: 67.85 ± 0.06	7.00
Sigma: 1.81			
Rwp%: 22.32		Sigma: 1.32	
		Rwp%: 8.64	
Clay minerals group – qualitative identification			
Illite		Illite	
Kaolinite		Kaolinite	
		Chlorite	

After exploring the available literature, a phenomenological estimation of hardness of principal minerals (observed by XRD tests on selected earths) has been made. For the qualitative considerations, Mohs scale values have been taken into account [66]. It is evident from Tab. 1 and Tab. 4 that average mineralogical composition hardness (evaluated by Mohs scale) is comparable.

3.4 Sample preparation

The two earths to be used to simulate plasters were disaggregated utilizing a rubber hammer. The 2-mm dry sieve-passing fraction was selected. In the case of TN, standard siliceous natural sand conforming to norm EN 196-1 and ISO 679:2009 was added.

Painted layers were prepared starting from rock fragments ground in an agate mortar. The resulting powder was sieved to select the 0.063-mm dry sieve-passing fraction. This was used to create coats of paint over the earthen tile support. In the case of FIN_P, the 0.125-mm dry sieve-passing fraction of a standard siliceous natural sand conforming to norm EN 196-1 and ISO 679:2009 was added.

All the materials were dried in an oven at 60 °C for about 12 h, which allows attaining constant weight. TN, VNF, FIN_Y and FIN_P materials were mixed with distilled water. The earths were placed in 7×7×15 cm^3 moulds. Support surfaces were moistened and FIN_Y and FIN_P were applied with a fine brush.

To properly balance the different constituents, different compositions of tiles and pictorial layers were considered. The compositions finally selected for tests are given in Tab. 5.

Tab.5 -Composition of tiles (TN and VNF) and pictorial layers (FIN_Y and FIN_P) expressed as weight fractions.

Designation	**Earth**	**Sand**	**Water**
TN	0.40	0.44	0.16
VNF	0.77	0	0.23
FIN_Y	0.54	0	0.46
FIN_P	0.39	0.26	0.35

32 samples prepared were given a single layer and 32 with three layers. In the samples with 3 layers, yellow and pink colours were interspersed in order to make the underlying pigment clearly visible in case of surface de-cohesion with the aim of evaluating the interaction between several pictorial layers.

Overall, 64 samples on 7×7×15 cm^3 tiles were prepared and divided into 8 groups with 8 samples each. The samples have different combinations of earth plaster, coating and number of surface layers as detailed in Tab. 6.

Tab. 6 - Summary table of the samples produced.

Samples group	Earth of plaster	N° of painted layers	Painted layers
A1 – A8	TN	1	FIN_Y
A9 – A16	VNF	1	FIN_Y
A17 – A24	TN	1	FIN_P
A25 – A32	VNF	1	FIN_P
AP1 – AP8	TN	3	FIN_Y FIN_P FIN_Y
AP9 – AP16	VNF	3	FIN_Y FIN_P FIN_Y
AP17 – AP24	TN	3	FIN_P FIN_Y FIN_P
AP25 – AP32	VNF	3	FIN_P FIN_Y FIN_P

The samples were kept at 23 ± 3 °C and relative humidity of 65 ± 5% for 4 months. Afterwards, surface cohesion and adhesion were evaluated by STT. The L^* a^* b^* colour coordinates by Konica Minolta CM-700 were measured according to UNI EN 15886:2010 [67].

For each sample, three measurements (repeated six times) within an area of approximately 1 cm^2 were evaluated. The final average value obtained for each sample is therefore the result of 18 measurements.

4. Accelerated aging

Accelerated aging was performed with the aim of simulating surface pulverization and loss of adhesion between pairs of pictorial layers as well as between pictorial layers and earthen support.

Based on the most important deterioration forms observed on-site and taking into account the meteorological dataset recorded, we simulated cycles of strong humidity and rapid drying by performing 2 wet-dry cycles (W-D) as well as the impact of sand particles carried by winds on the earthen surfaces by performing 2 sandblasting cycles (SB). This order W-D and

SB has been chosen to have the worst condition. Indeed, in Pachacamac, humidity is very high throughout the year, while winds become intense only in some months.

Several experiments have been designed to identify the conditions approaching real weathering. The W-D cycles were carried out in an Angelantoni DY 250 climatic chamber, while an home-made device was fabricated *ad hoc* for the sandblasting cycles based on the work of Atzeni et al. [49,50].

At the end of each W-D or SB cycle, pictures of the exposed earthen surfaces were observed and subjected to STT and colorimetric measures to evaluate ΔE in accordance with UNI EN 15886:2010:

$$\Delta E^*_{2,1} = \sqrt{(L^*_2 - L^*_1)^2 + (a^*_2 - a^*_1)^2 + (b^*_2 - b^*_1)^2}$$

4.1 W-D cycles

Several preliminary tests have been designed for the W-D cycles. In particular, the protocols tested were:

Protocol 1: the samples were introduced into the climatic chamber at a temperature of 20° C and RH of 30%. RH values were increased each 24 h reaching progressively 50%, 75%, 90% and 98%. When 98% RH has been reached, the temperature has been increased by 10°C every 24 h. When 50°C has been reached, this condition was maintained for 24 h and then the RH was brought to 11%. Even though this procedure has been repeated 4 times, the produced aging is too slow and soft.

Protocol 2: the samples were introduced into the climatic chamber at a temperature of 20°C and RH of 30%. RH values were increased each 12 h reaching progressively 50%, 75%, 90% and 98%. When 98% RH has been reached, the temperature has been increased by 10°C every 12 h. When 50°C has been reached, this condition was maintained for 12 h and then the RH was brought to 11%. Even though this procedure has been repeated 8 times, the produced aging is too slow and soft.

Protocol 3: the samples were sprayed for 10 s in the two major faces with distilled water using nebulizing nozzles 50 cm away from each surface. In the same manner, the

sides of the sample were sprayed for 5 seconds. In this way, moistening is visually homogeneous over the entire surface. Water absorbed by samples at the end of the spraying time was found to be 8.4 g ± 0.5 g. Moistened samples were placed in a climatic chamber previously conditioned at 50 °C and RH of about 11% for 2 h to induce the strong heating of surfaces and then their rapid drying. Once extracted from the climatic chamber, the samples were left at T = 23 ± 3 °C and RH = 65 ± 5% for 4 h. Every sample was exposed twice to the W-D cycle. However, these cycles degraded the samples too rapidly.

Protocol 4: the samples were sprayed for 5 s with distilled water using nebulizing nozzles 50 cm away from the painted surface. Water absorbed by samples at the end of the spraying time was found to be 1.5 ± 0.2 g. Moistened surfaces appeared homogeneous. Moistened samples were placed in a climatic chamber previously conditioned at 50 °C and RH of about 11% for 2 h to induce the strong heating of surfaces and then their rapid drying. Once extracted from the climatic chamber, the samples were left at T = 23 ± 3 °C and RH = 65 ± 5% for 4 h. Every sample was exposed twice to the W-D cycle. The obtained samples show a deterioration characterised by the typical features (observed by STT method) usually due to RH variation. For this reason, the protocol 4 was chosen for the accelerated aging and after SB cycles were carried out.

4.2 SB cycles

Sandblasting cycles were performed according to the methods illustrated in Atzeni et al. [49,50].

The experimental apparatus consists of: (a) 24 L electric compressor for generating dry air flow at constant temperature and pressure. The internal pressure of the compressor chamber is set at 4.5 bar, while the outlet pressure is adjustable through a pressure reducer; (b) sandblasting gun with 6 mm nozzle for the flow of air and abrasive with a 6 mm hole for the attachment of a tube that allows the suction of the abrasive; (c) 20 cm diameter tube to confine the jet; (d)system for collecting the abrasive in output; (e) sample holder for the arrangement of the facsimile perfectly aligned with the abrasive jet.

A quartz sand was used as the abrasive. Sand particles had nominal average diameter of 300 μm within the range typically undergoing saltation [68,69] in *Pachacamac*.

The optimal nozzle-sample distance of the nozzle and the optimal outlet pressure of the abrasive jet were identified by studying the radial air speed profiles within the jet. Air speed was measured using Hot Wire Anemometer HHF-SD1 by Omega placed at 18 and 28 cm from the nozzle. Three different airflow exit pressures, namely 1, 2 and 3 bar, were considered. The obtained results are summarised in Fig. 4. It can be seen that the air speed, which is maximum along the jet axis, reduces by half as the nozzle distance increases from 18 to 28 cm.

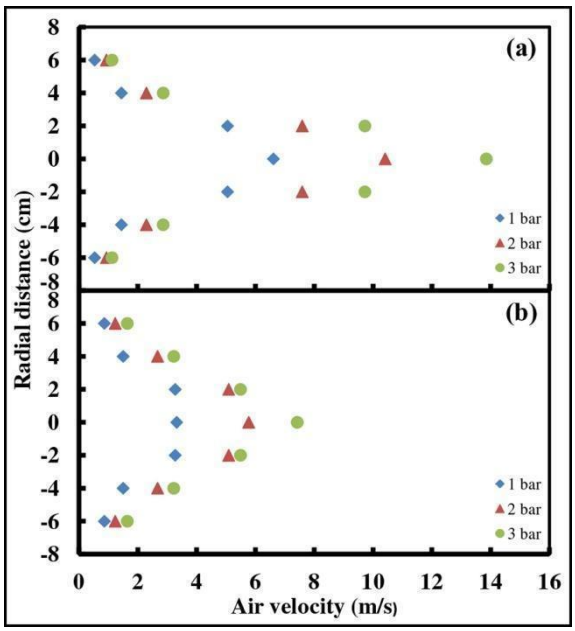

Fig. 4 - Velocity profiles obtained at 18 cm (a) and 28 cm (b) for the three pressures.

SB experiments were carried out with the nozzle placed at 28 cm from the surface and an airflow pressure of 1 bar. This results in a quite uniform air speed all over the sample area. Under these working conditions, the measured airflow speed was about 3.32 m s^{-1}. The earthen surface was exposed to the abrasive jet for 5 s, then monitored with STT, and exposed again for 5 s. Accordingly, the earthen surface was hit by 2.77 ± 0.3 g s^{-1}, i.e. about 13.85 g of sand during each 5-s long exposure time. Since sand particle are about 300 μm in diameter and have specific weight of about 2.5 g cm^{-3}, approximately 1.64×10^{6} sand particles reached the sample surface. Every sample was exposed twice to the SB cycle.

5. Results and discussion

5.1 Observations and measurements before accelerated aging on prepared samples

On the macroscopic scale, every series showed samples with fairly homogeneous properties. In general, all the yellow and single-layer coatings display a slightly rough surface, with some marks left by the brush. Pink surfaces appear rougher due to the presence of sand. Roughness is also clearly detected on yellow surfaces in multi-layered samples due to the direct contact with the surface of the pink coating underneath.

After 4 months, the surfaces constituted by FIN_P were found to be less cohesive because of the presence of sand and the consequent decrease in clay-binder fraction that made them more susceptible to microcracking (AP 17 sample in Fig. 5a). Particularly, surfaces AP17-AP24 started showing the first signs of degradation and superficial hairline cracks appeared. The reason lies in the very strong sensitivity to small variations in RH% that cause swelling of the smectitic clay fraction of support TN. The pictorial layers deform differently due to diverse nature, stressing each other.

STT values measurements performed after 4 months were the reference point for evaluating, respectively, the variation of surface cohesion and adhesion and the visual change induced by aging.The initial removed materials (BAA) for each type of sample are shown in the Tab. 7.

Tab. 7 - Summary table of the colour coordinates before (L*1 - a*1 - b*1) and after accelerated aging (L*2 - a*2 - b*2), ΔE and the average of removed material by STT. BAA: Before Accelerated aging; 1 W-D: 1° wet-dry cycle; 2° W-D: 1° wet-dry cycle; 1 SB: 1° sandblasting cycle; 2 SB: 2° sandblasting cycle. DT: degradation type for lab samples (F: flaking - P: pulverisation). CD: archaeological samples comparable to lab ones, relative deterioration and STT values. The comparable data are reported in bold.

Samples group	**L^*_1** / **L^*_2**	**a^*_1** / **a^*_2**	**b^*_1** / **b^*_2**	**ΔE**	**BAA (%)**	**1 W-D (%)**	**2 W-D (%)**	**1 SB (%)**	**2 SB (%)**	**DT**	**CD (%)**
A1 - A8	64.75	10.89	32.79	5.20	0.38	0.87	1.18	**14.80**	30.16	F	Vermillon red (**13.70%**) F
	65.18	9.25	27.92								
A9 - A16	64.65	11.36	33.87	3.80	0.45	0.78	2.10	8.76	30.93	F	
	66.73	10.22	30.92								
A17 - A24	60.04	13.52	19.98	1.30	3.47	37.00	63.73	100.00	--	P	
	59.18	14.17	20.75								
A25 - A32	61.21	13.86	20.11	2.21	2.25	7.84	18.72	58.58	100.00	P	
	63.25	13.61	20.82								
AP1 - AP8	68.13	9.32	32.45	2.42	1.21	3.64	7.76	10.83	**15.14**	F	Vermillon red (**13.70%**) F
	69.43	8.82	30.49								
AP9 - AP16	68.48	9.20	32.68	2.76	0.71	1.77	2.20	8.15	**14.49**	F	
	69.81	8.62	30.34								
AP17 - AP24	60.18	14.23	20.82	1.94	1.60	5.86	15.43	**27.58**	47.49	P	Pale yellow (**26.93%**) P
	61.93	13.78	20.71								
P25 - AP32	60.76	14.27	20.33	2.01	2.51	7.72	10.96	**26.16**	46.60	P	
	62.52	13.70	20.34								

5.2 Observations and measurements after accelerated aging on prepared samples

The deterioration forms observed have been described by subdividing the pathologies observed in the two types of cycles performed, while the evaluation of adhesion and surface cohesion measured by STT will be discussed before for *in situ* inspections.

5.2.1 Wet-dry cycles

W-D cycles are responsible for most of peeling, flaking and cracking. Peeling and flaking of the surface occur due to the loss of adhesion of the pictorial layers of the material, while cracking depends on swelling. For these reasons, they particularly affect multi-layered samples.

In particular, in the first phase of W-D cycles related to sample damping, a strong sensitivity to water was observed. Bulges of different diameters (the sizes observed range from 0.3 cm to 1.3 cm) formed on the surfaces, denoting the detachment of the superficial layer from the underlying one (Fig. 5b and 5c). Water absorbed by clays and interposed between coating grains causes a volume increase and the consequent detachment of the superficial pictorial layer. The phenomenon is more frequent for AP1-AP8 and AP9-AP16 samples, which are different in type of support used, but both contain FIN_Y as surface layer in direct contact with FIN_P. These samples exhibit weaker adhesion between the yellow and the underlying pink surfaces. The lower cohesion of FIN_P does not allow the yellow layer to adhere effectively and in the absence of obstacles to its expansion, it deforms and detaches (Fig. 5b). In the rapid evaporation phase, for yellow surfaces, the dimension of bulges decreases until external layer returns parallel and in contact with the pink coat. However, when contraction takes place, the underlying pink layer is already completely dry. These two layer are only in contact without any adhesion. The flake detachment, in the case of larger bulges, is revealed by the STT which, through the superficial peeling, no longer removes the grains but the entire surface layer.

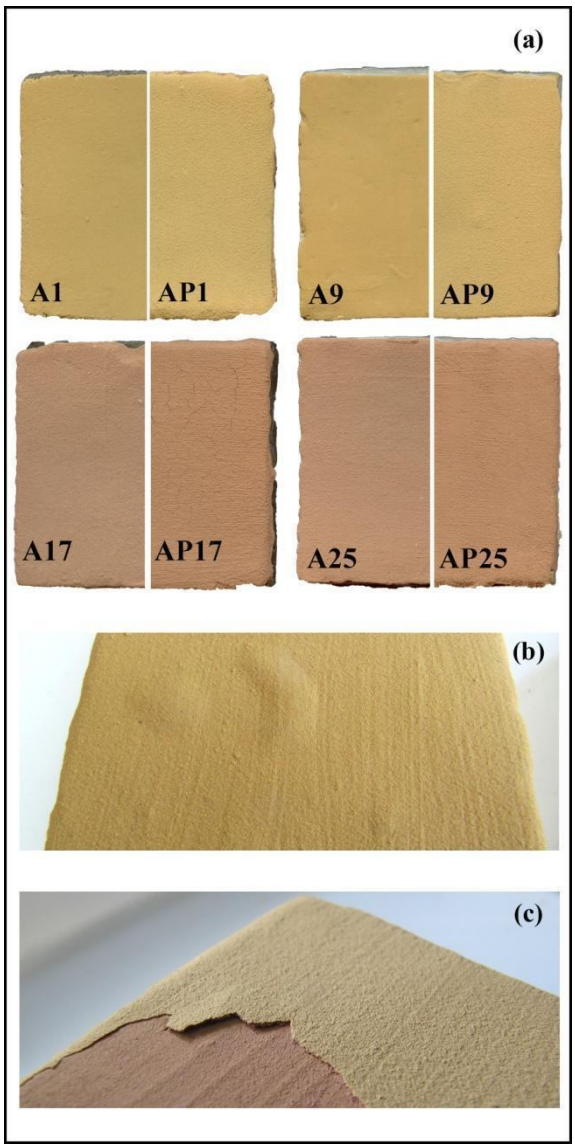

Fig. 5 - (a) Laboratory samples before accelerated aging. surfaces AP17-AP24 samples started showing the first signs of degradation and superficial hairline cracks appeared. Larger bulges in (b) and subsequent flake detachment (c) after wet-dry cycles in AP4 sample.

Surface microcracking appears or intensifies after the W-D cycles. The phenomenon originates from the different expansion and contraction of the diverse materials following imbibition and subsequent rapid drying. The intensity of microcracking, referring to the extension of the phenomenon on the surface and the thickness of microcracks, is greater in the supports AP1-AP8 and AP17-AP24, both multilayer groups with TN earth plaster.

The observed degradation is similar to the one obtained with the wet-dry cycles carried out by Ferron et al. [48] and Ogura et al. [51], which result in a reduced surface cohesion and an intensified microcracking.

5.2.2 Sandblasting cycles

Erosion increased macroscopic surface roughness and the loss of cohesion in the surface layer in each group of samples. Surface micro-craters were generated by particle impacts and they represent the points where aging process induces further coating cracking.

5.2.3 Colorimetric measurements

After accelerated aging, the colour change of the surfaces was measured by colourimetry. Tab. 7 shows the colour coordinates (L^*, a^*, b^*) and the ΔE.

In general, substrates with only one layer (A1-A8, A9-A16, A17-A24 and A25-A32) tend to have a higher ΔE, while multilayered substrates show greater homogeneity. Deteriorated monolayered samples exhibit, indeed, surface portions of the support which are characterised by a very different colour. Contrarily, multilayered samples after deterioration expose the underlyinglayer of the painted surface, which is more similar to the first layer (external).

Samples A17-A24 showed the smallest ΔE. This can be probably ascribed to the fact that not all the aging cycles could be completed since they already underwent significant degradation after the first erosion cycle.

All samples are more lightweight after aging, as shown by the increase in the L^* parameter. As demonstrated by Ogura et al. [51], mechanical degradation produces important colorimetric variations, especially in the case of erosion cycles. In particular, the studies carried out showed a discolouration of the surfaces ascribable to the erosion induced by sand particles carried by wind, in agreement with what was also found in this study. The only case in which L^* decreases is for samples A17-A24. It is due to the high degree of degradation shown by the pictorial layer, which exhibits the darker TN support. Finally, the higher pulverisation leads to an increase in surface roughness with a consequent decrease in L^* values.

5.2.4 Measurement by STT

STT was performed before accelerated aging and after each cycle. The average material loss was evaluated over 3 tapes per sample after each cycle. The results obtained are shown in Tab. 7.

Within group A, only the samples with FIN_Y (A1-A8 and A9-A16) have completed the

entire aging process. For A17-A24 and A25-A32 subgroups, the cycles were interrupted at the second and third stages because of the extensive degradation undergone.

No significant difference was observed between subgroups A1-A8 and A9-A16. Both subgroups show an increase in the rate of degradation kinetics with erosion cycles. The subgroups that mostly degrade are those with FIN_P. These surfaces contain fine sand to reduce the cracking processes during drying. For samples which have a greater quantity of sand, it has been observed that the cohesion decreases due to the minor quantity of binding phase into the prepared system. Consequently, thermal-hygrometric and mechanical stresses cause a remarkable deterioration.

In subgroup A17-A24, the obtained values indicate that W-D cycles (the only ones performed on this subgroup) caused very severe deterioration of the coating. After the first cycle in the climatic chamber, FIN_P was removed very easily over a great area examined (37%), demonstrating a total absence of cohesion and adhesion with the support. The TN support is, indeed, highly susceptible to thermo-hygrometric variations induced by the W-D cycles, which solicits the FIN_P layer. Furthermore, the presence of a single layer increases the amount of water that reaches the earthen support and, consequently, the amount of TN soil involved in the swelling process. Moreover, the importance of the support is emphasised when the degradation obtained in this subgroup (A17-A24) is compared with that of the subgroup A25-A32 constituted by the same FIN_P on the surface, but with VNF support. For A25-A32, it is possible to note that the surfaces are more resistant to wet-dry cycles due to the less swelling of the substrate.

Multi-layered AP samples show greater stability with respect to the overall aging process compared to those of group A monolayer (Tab. 7). The groups consisting of multi-layered surface FIN_Y (AP1-AP8 and AP9-AP16) once again appear to be the most resistant to both W-D and SB cycles. However, it is possible to note a higher value reached at the end of the second cycle with respect to the A samples due to a high roughness surface given the presence of the underlying FIN_P layer. Roughness as well as surface defects greatly influence the test results, making the surface more prone to be removed. Despite a lower resistance to W-D cycles, at the end of the entire aging process, there is still a smaller amount of coating removed since the sandblasting cycles are much less effective than that in the case of group A.

For samples with FIN_P (AP17-AP24 and AP25-AP32) in the surface, W-D cycles are

less damaging. It is possible to see in Tab. 7 that the obtained results for AP17-AP24 and AP25-AP32 are quite similar to each other, suggesting that the presence of the multilayer has a greater influence than the difference in earthen substrates.

For multilayer FIN_Y (AP1-AP8 and AP9-AP16) samples, W-D and SB cycles caused similar damage step by step due to the fact that FIN_Y upper layer is particularly cohesive (especially regarding monolayer FIN_P), therefore it reduces the pulverization effect by protecting the underlying layer which is more sensitive (FIN_P). After W-D cycles, the surface is characterised by micro-cracks growth which increase their dimension. Their merge gives rise to flakes which exfoliate exposing a new layer to damage process (Fig. 6).

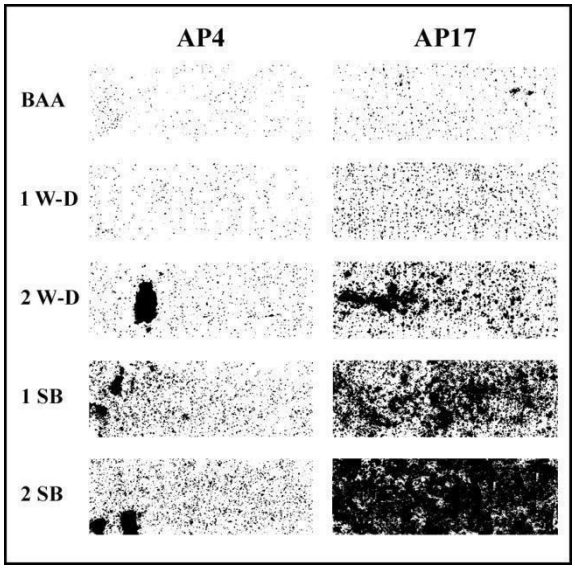

Fig. 6 - Tapes of AP4 and AP17 samples during accelerated aging cycles. It is possible to note the loss of adhesion between layers, evidenced by flake detachment, in sample AP4 and the loss of surface cohesion manifested by pulverisation in sample AP17.

The reported results show that artificial weathering is comparable with real one observed on the archaeological site. Indeed, in both cases, it is possible to note that the minor loss of external layer (flakes) takes place for earth with a greater quantity of quartz, while pulverization is higher for systems with more equal proportions between quantity of minerals fractions (quartz + clays). Through phenomenological observations and XRD data, it is possible to note that the percentage of minerals with Mohs hardness greater than 5 in the pulverised samples is lower for both archaeological (49.5% for pale yellow vs. 68.1% for vermillion red) and reproduced samples (83% in FIN_P vs. 93.40% in FIN_Y).

Particularly, as shown in Tab. 7, a remarkable agreement has been observed between archaeological surfaces vermillon red and monolayer A1-A8 after 1 SB and multilayer samples called AP1-AP8 and AP9-AP16 at the end of 2 SB. STT exhibits comparable results of removed materials (about 14-15%) and deterioration type (flaking).

Moreover, for pale yellow (archaeological) samples, pulverisation results are comparable with those obtained for AP17-AP24 and AP25-AP32 (experimental) samples at the third cycle; estimated between 26 and 27%.

For A9-A16, A17-A24 and A25-A32, it is not possible to compare STT values which result extremely different to those measured for the archaeological surfaces studied.

Overall, different samples have been prepared for the application of consolidant materials and consequent conservation strategies and design.

Conclusions

This work presents a materials accelerated aging procedure for reproducing weathering deterioration observed on painted surfaces of *Pachacamac Templo*. It allows to obtain deteriorated samples which can be used for understanding weathering conditions and testing new consolidants.

Thermal hygrometric variation and wind erosion are the typical deterioration causes noticed in the study area. For this reason, wet-dry and sandblasting cycles are used in lab for obtaining accelerated deteriorated samples prepared by using raw materials composition with similar mechanical and composition properties.

In both archaeological and lab samples, weathering is estimated by the application of STT which allows estimating removed material layers. According to similar mineralogical compositions, the comparison between archaeological and lab samples shows that damage observed in A1-A8, AP1-AP8 and AP9-AP16 is similar to that in vermillion red and damage observed in AP17-AP24 and AP25-AP32 is close to that in pale yellow.

This result represents a step forward to formalise simple guidelines for artificial damaging aimed at studying new consolidating materials and approaches.

Acknowledgements

We gratefully acknowledge Sardinia Regional Government for the financial support for the PhD scholarship (P.O.R. Sardegna F.S.E. Operational Programme of the Autonomous Region of Sardinia, European Social Fund 2007-2013 - Axis IV Human Resources, Objective l.3, Line of Activity l.3.1.)". We would like to thank all the staff of the Archaeological Sanctuary of Pachacamac, in particular the Director Denise Pozzi-Escot and the archaeologist Gianella Pacheco, for sharing environmental data, information and consenting to the holding of the Templo Pintado. The financial support of Fondazione di Sardegna, project F72F20000360007, is also gratefully acknowledged.

References

[1] R. Anger, L. Fontaine, Batir en terre, du grain de sable à l'architecture, Belin, Paris, 2009.

[2] UNESCO, World Heritage, Inventory of earthen Architecture, 2012. http://whc.unesco.org/en/earthen-architecture/.

[3] M. Correia, L. Guerrero, A. Crosby, Technical strategies for conservation of Earthen archaeological architecture, Conserv. Manag. Archaeol. Sites. 17 (2015) 224–256. https://doi.org/10.1080/13505033.2015.1129799.

[4] A.A. Balderrama, The Conservation of Earthen Architecture, Getty Conserv. Inst. Newsl. 16 (2001) 4–11.

[5] H. Houben, A.A. Balderrama, Our Earthen Architectural Heritage : Materials Conservation Raw Earth Construction, MRS Bull. 29 (2004) 338–341. www.mrs.org/publications/bulletin.

[6] UNESCO, Earthen architecture in today's world, in: E. Lazare, J. Thierry (Eds.), Proc. UNESCO Int. Colloq. Conserv. World Herit. Earthen Archit. Archit. 17-18 December 2012, United Nations Educational, Scientific and Cultural Organization, 2013. http://whc.unesco.org/en/series/.

[7] L. Rainer, The conservation of decorated architectural surfaces, Getty Conserv. Inst. Newsl. 25 (2010) 1–9. http://getty.edu/conservation/publications_resources/newsletters/25_2/feature.html.

[8] F.G. Matero, The Conservation of Plasters in Earthen Archeological Sites, in: Conserv. Earthen Archit., 1999: pp. 59–62.

[9] L. Guerrero, M. Correia, H. Guillaud, Conservación del patrimonio arqueológico construido con tierra en iberoamérica., Conserv. Ibero-American Archaeol. Herit. Built Earth. 25 (2012) 210–225. http://ezproxy.uniandes.edu.co:8080/login?url=http://search.ebscohost.com/login.aspx?direct=true&db=fua&AN=91642368&lang=es&site=eds-live&scope=site.

[10] F. Matero, Conservation and Management of Archaeological Sites Mud Brick Metaphysics and the Preservation of Earthen Ruins Mud Brick Metaphysics and the Preservation of Earthen Ruins, Conserv. Manag. Archaeol. Sites. 17 (2016) 209–223. https://doi.org/10.1080/13505033.2015.1129798.

[11] UNESCO, World Heritage List, (n.d.). http://whc.unesco.org/en/list/.

[12] World Congress Terra 2016, The Lyon Declaration, in: Terra Lyon 2016 Actes / Proc. / Actos, 2017.

[13] UNESCO, World Heritage Earthen Architecture Programme (WHEAP), (n.d.). https://whc.unesco.org/en/earthen-architecture/.

[14] UNESCO, List of World Heritage in Danger, (n.d.). https://whc.unesco.org/en/danger/.

[15] J. Barton, 3D laser scanning and the conservation of earthen architecture: A case study at the UNESCO World Heritage Site Merv, Turkmenistan, World Archaeol. 41 (2009) 489–504. https://doi.org/10.1080/00438240903112518.

[16] M. Oliver, A. Mesbah, Behaviour of ancient and new structures made out of raw earth, Trans. Built Environ. 4 (1998). https://www.witpress.com/Secure/elibrary/papers/STR93/STR93042FU.pdf.

[17] L.F. Guerrero Baca, Revoques para la conservación de obras arqueológicas de tierra en Mexico, in: T. Joffroy, H. Guillard, C. Sadozaï (Eds.), Terra Lyon 2016 Actes / Proc. / Actos, CRATerre, Villefontaine, 2017: pp. 94–98.

[18] G. Chiari, Conservazione in situ di fregi dipinti su mattone crudo, in: Archeol. Recuper. e Conserv., Istituto p, Nardini, Firenze, 1993: pp. 169–183.

[19] H. Barnard, W.Z. Wendrich, A. Winkels, J.E.M.F. Bos, B.L. Simpson, R.T.J. Cappers, The preservation of exposed mudbrick architecture in Karanis (Kom Aushim), Egypt, J. F. Archaeol. 41 (2016) 84–100. https://doi.org/10.1080/00934690.2015.1131109.

[20] A. Weyer, P. Roig Picazo, D. Pop, J. Cassar, A. Özköse, J. Vallet, I. Srša, EwaGlos – European Illustrated Glossary of Conservation Terms for Wall Paintings and Architectural Surfaces, 2015.

[21] N. Hauptvogel, D. Geyer, S. Simon, B. Kebede Amare, Consolidation of burned earthen plaster, Grat Be' Al Gebri, Ethiophia, in: Terra Lyon 2016 Actes / Proc. / Actos, 2017: pp. 192–198.

[22] A. Ferron, F.G. Matero, A Comparative Study of Ethyl-silicate–based Consolidants on Earthen Finishes, J. Am. Inst. Conserv. 50 (2013) 49–72. https://doi.org/10.1179/019713611804488964.

[23] G. Chiari, Consolidation of adobe with ethyl silicate: control of long-term effects using SEM, 5th Int. Meet. Expert. Conserv. Earthern Archit. Rome, 22-23, X, 1987. (1987) 25–32.

[24] A. Bourgès, M. Tiennot, J.-D. Mertz, A. Liégey, A. Bouquillon, Review of earthen material consolidation with ethyl silicate, in: T. Joffroy, H. Guillard, C. Sadozaï (Eds.), Terra Lyon 2016 Actes / Proc. / Actos, CRATerre, Villefontaine, 2017: pp. 104–107.

[25] R.J. Carr, Evaluation of Adhesive Binders for the Preservation of In-Situ Aboriginal Surface Finishes at Mesa Verde National Park Evaluation of Adhesive Binders for the Preservation of In-Situ Aboriginal Surface Finishes at Mesa Verde National Park, University of Pennsylvania, 2002.

[26] W. Chen, Y. Zhang, J. Zhang, P. Dai, Consolidation effect of composite materials on earthen sites, Constr. Build. Mater. 187 (2018) 730–737. https://doi.org/10.1016/j.conbuildmat.2018.07.239.

[27] G. Chiari, Chemical Surface Treatments and Capping Techniques of Earthen Structures: A Long- Term Evaluation, in: 6th Int. Conf. Conserv. Earthen Archit. Adobe 90, 1990: pp. 267–273.

[28] X. He, M. Xu, H. Zhang, B. Zhang, B. Su, An exploratory study of the deterioration

mechanism of ancient wall-paintings based on thermal and moisture expansion property analysis, J. Archaeol. Sci. 42 (2014) 194–200. https://doi.org/10.1016/j.jas.2013.10.035.

[29] M. Sun, J. Zou, H. Zhang, B. Zhang, Measurement of reversible rate of conservation materials based on gel cleaning approach, J. Cult. Herit. 16 (2015) 719–727. https://doi.org/10.1016/j.culher.2014.11.006.

[30] M. Sun, J. Wang, H. Zhang, B. Zhang, Z. Fan, B. Su, Measurement of the reversible rate of conservation materials for ancient murals, J. Cult. Herit. 16 (2015) 49–56. https://doi.org/10.1016/j.culher.2014.01.010.

[31] I Comité de Conservación del ICOM, Principios Para La Preservación, Conservación Y Restauración De Pinturas Murales (2003), 2 (2003) 6. http://www.icomos.org/charters/wallpaintings_sp.pdf.

[32] E. Kopelson, Analysis and consolidation of architectural plasters from Çatalhöyük, Turkey, University of Pennsylvania, 1996.

[33] B. Lubelli, R.P.J. Van Hees, T.G. Nijland, J. Bolhuis, A new method for making artificially weathered stone specimens for testing of conservation treatments, J. Cult. Herit. 16 (2015) 698–704. https://doi.org/10.1016/j.culher.2015.01.002.

[34] M.I.G. Beas, Traditional architectural renders on earthen surfaces, (1991) 261.

[35] A. Ferron, The Consolidation of Earthen Surface Finishes : A Study of Disaggregating Plasters at Mesa Verde National Park, University of Pennsylvania, 2007.

[36] M. Ban, A. Baragona, E. Ghaffari, J. Weber, A. Rohatsch, Artificial aging techniques on various lithotypes for testing of stone consolidants, Sci. Art A Futur. Stone. Proc. 13th Int. Congr. Deterior. Conserv. Stone. (2016) 253–260.

[37] P. Tiano, E. Pecchioni, Invecchiamento artificiale di materiali lapidei, in: Giorn. Di Stud. Camere Clim. Od Ambient. Nella Ric. Appl. - CNR - C.S. “Cause Deperimento e Metod. Conserv. Opere d’Arte,” Firenze, 1990: pp. 37–42.

[38] H. Bansa, Accelerated Aging Tests in Conservation Research: Some Ideas for a Future Method, Restaurator. 13 (1992) 114–137. https://doi.org/10.1515/rest.1992.13.3.114.

[39] F. Sitzia, C. Lisci, J. Mirão, Accelerate ageing on building stone materials by simulating daily, seasonal thermo-hygrometric conditions and solar radiation of Csa Mediterranean climate, Constr. Build. Mater. 266 (2021) 121009. https://doi.org/10.1016/j.conbuildmat.2020.121009.

[40] K.A. Heathcote, Durability of earthwall buildings, Constr. Build. Mater. 9 (1995) 185–189. https://doi.org/10.1016/0950-0618(95)00035-E.

[41] J. Vargas Neuman, E. Heredia Zavoni, J. Bariola Bernales, P.K. Mehta, Preservación de las construcciones de adobe en areas lluviosas, Lima, PE; mayo 1986, Lima, 1986.

[42] F.O. Ogunye, H. Boussabaine, Diagnosis of assessment methods for weatherability of stabilised compressed soil blocks, Constr. Build. Mater. 16 (2002) 163–172. https://doi.org/10.1016/S0950-0618(02)00004-1.

[43] P. Walker, R. Keable, J. Martin, V. Maniatidis, Rammed earth: design and construction guidelines, PublisherIHS BRE, 2005.

[44] M. Mattone, Intonaci in terra e gesso per la protezione delle costruzioni in terra cruda, in: Construcción Con Tierra. Tecnol. y Arquit. Congr. Arquit. Tierra En Cuenca Campos, 2011: pp. 315–322. http://www5.uva.es/grupotierra/publicaciones/digital/libro2011/2011_9788469481073_p315- 322_mattone.pdf.

[45] F.P. Torgal, S. Jalali, Eco-efficient Construction and Building Materials, Springer-Verlag London, 2011. https://doi.org/10.1017/CBO9781107415324.004.

[46] J.C. Morel, Q.B. Bui, E. Hamard, Weathering and durability of earthen material and structures, in: Mod. Earth Build. Mater. Eng. Constr. Appl., 2012: pp. 282–303. https://doi.org/10.1533/9780857096166.2.282.

[47] C.T.S. Beckett, P.A. Jaquin, J.C. Morel, Weathering the storm: A framework to assess the resistance of earthen structures to water damage, Constr. Build. Mater. 242 (2020) 118098. https://doi.org/10.1016/j.conbuildmat.2020.118098.

[48] A. Ferron, F. Matero, The Consolidation of Earthen Surface Finishes : Developing a Protocol for Treatment Evaluation at Mesa Verde National Park, in: Terra 2008 Proc. 10th Int. Conf. Study Conserv. Earthen Archit. Heritage, Bamako, Mali, Febr. 1–5,

2008, 2008.

[49] C. Atzeni, F. Bodano, U. Sanna, N. Spanu, Surface strength: definition and testing by a sand impact method, J. Cult. Herit. 7 (2006) 201–205. https://doi.org/10.1016/j.culher.2006.05.002.

[50] C. Atzeni, G. Pia, U. Sanna, N. Spanu, Surface wear resistance of chemically or thermally stabilized earth-based materials, Mater. Struct. 41 (2008) 751–758. https://doi.org/10.1617/s11527-007-9278-1.

[51] D. Ogura, T. Hase, Y. Nakata, A. Mikayama, S. Hokoy, H. Takabayashi, K. Okada, B. Su, P. Xue, Influence of Environmental Factors on Deterioration of Mural Paintings in Mogao Cave 285, Dunhuang, in: J.M.P.Q. Delgado (Ed.), Case Stud. Build. Rehabil. Build. Pathol. Rehabil., Porto, 2021: pp. 105–159. http://www.springer.com/series/10019.

[52] J.A. Ramos Giraldo, Santuario de Pachacámac: cien años de arqueología en la costa central, Editorial, 2011.

[53] G. De La Vega, Comentarios reales. Origen e Historia de los Incas del Peru (1609), Mercurio, Lima, 1970.

[54] D. Pozzi-Escot, G. Pacheco, C.R. Uceda, Pachacamac: Templo Pintado - Conservación e Investigación, Ministerio, Lima, 2013.

[55] D. Pozzi-Escot, Pachacamac: Conservación en arquitectura de tierra, 2014.

[56] D. Pozzi-Escot, Santuario arqueológico Pachacamac, Lima, 2016.

[57] F.J. Régulo G., Poder religioso , crisis y prosperidad en Pachacamac : del Horizonte Medio al Intermedio, Bull. l ' Inst. Français d ' Études Andin. 33 (2004) 1–46.

[58] G. Marcone Flores, Los murales del Templo Pintado o Relación entre el Santuario de Pachacamac y la iconografía tardía de la Costa Central Peruana, An. Del Mus. Am. 11 (2003) 57–80.

[59] W.S. Chepil, Dynamics of wind erosion: I.Nature of movement of soil by wind, Soil Sci. 60 (1945) 305–320.

[60] S. Malpartida Tuncar, Estudio de algunas propiedades físicas de enlucidos de barro

consolidados con mucílago de tuna, agar agar y gelatina, Universidad Nacional de Ingeniería, Lima, Peru, 2015. http://cybertesis.uni.edu.pe/handle/uni/4536.

[61] ASTM, ASTM 4214-07 - Standard Test Methods for Evaluating the Degree of Chalking of Exterior Paint Films, (2015).

[62] M. Drdácký, J. Lesák, K. Niedoba, J. Valach, Peeling tests for assessing the cohesion and consolidation characteristics of mortar and render surfaces, Mater. Struct. Constr. 48 (2015) 1947–1963. https://doi.org/10.1617/s11527-014-0285-8.

[63] A.R. Young, The Rietveld Method, Oxford Science Pubblication, New York, 2000.

[64] D.M. Moore, R.C. Reynolds, X-ray Diffraction and the Identification and Analysis of Clay Minerals, Oxford University Press, New York, 1997.

[65] V.E. García-Vera, M. Lanzón, Physical-chemical study, characterisation and use of image analysis to assess the durability of earthen plasters exposed to rain water and acid rain, Constr. Build. Mater. 187 (2018) 708–717. https://doi.org/10.1016/j.conbuildmat.2018.07.235.

[66] A. Szymański, M.J. Szymański, Hardness estimation of minerals, rocks and ceramic materials (Materials Science Monographs), Elsevier, 1990.

[67] UNI EN 15886:2010, Conservation of cultural property - Test methods - Colour measurement of surfaces, (2010).

[68] D. Camuffo, Controlling the aeolian erosion of the Great Sphinx, Stud. Conserv. 38 (1993) 198–205. https://doi.org/10.2307/1506380.

[69] D. Camuffo, Physical weathering of stones, Sci. Total Environ. 167 (1995) 1–14. https://doi.org/10.1016/0048-9697(95)04565-I.